International Journal of Solids and Structures 47 (2010) 665–677

Contents lists available at ScienceDirect

International Journal of Solids and Structures

journal homepage: www.elsevier.com/locate/ijsolstr

An anisotropic elastic–viscoplastic model for soft clays

Zhen-Yu Yin [a,b,*], Ching S. Chang [a], Minna Karstunen [c], Pierre-Yves Hicher [b]

[a] Department of Civil and Environmental Engineering, University of Massachusetts, Amherst, MA 01002, USA
[b] Research Institute in Civil and Mechanical Engineering, GeM UMR CNRS 6183, Ecole Centrale de Nantes, BP 92101, 44321 Nantes Cédex 3, France
[c] Department of Civil Engineering, University of Strathclyde, John Anderson Building, 107 Rottenrow, Glasgow G4 0NG, UK

ARTICLE INFO

Article history:
Received 29 March 2009
Received in revised form 9 November 2009
Available online 15 November 2009

Keywords:
Anisotropy
Clays
Creep
Constitutive models
Strain-rate
Viscoplasticity

ABSTRACT

Experimental evidences have shown deficiencies of the existing overstress and creep models for viscous behaviour of natural soft clay. The purpose of this paper is to develop a modelling method for viscous behaviour of soft clays without these deficiencies. A new anisotropic elastic–viscoplastic model is extended from overstress theory of Perzyna. A scaling function based on the experimental results of constant strain-rate oedometer tests is adopted, which allows viscoplastic strain-rate occurring whether the stress state is inside or outside of the yielding surface. The inherent and induced anisotropy is modelled using the formulations of yield surface with kinematic hardening and rotation (S-CLAY1). The parameter determination is straightforward and no additional experimental test is needed, compared to the Modified Cam Clay model. Parameters determined from two types of tests (i.e., the constant strain-rate oedometer test and the 24 h standard oedometer test) are examined. Experimental verifications are carried out using the constant strain-rate and creep tests on St. Herblain clay. All comparisons between predicted and measured results demonstrate that the proposed model can successfully reproduce the anisotropic and viscous behaviours of natural soft clays under different loading conditions.

1. Introduction

Deformations and strength of soft clay is highly dependent on the rate of loading, which is an important topic of geotechnical engineering. The time-dependency of stress–strain behaviour of soft clays has been experimentally investigated through one-dimensional and triaxial test conditions by numerous researchers (i.e., Bjerrum, 1967; Vaid and Campanella, 1977; Mesri and Godlewski, 1977; Graham et al., 1983; Leroueil et al., 1985, 1988; Nash et al., 1992; Sheahan et al., 1996; Rangeard, 2002; Yin and Cheng, 2006).

The most popular models for time-dependency behaviour of soft soils, based on Perzyna's overstress theory (Perzyna, 1963, 1966), can be classified into two categories:

(1) Conventional overstress models, assuming a static yield surface for stress state within which only elastic strains occur (e.g., Adachi and Oka, 1982; Shahrour and Meimon, 1995; Fodil et al., 1997; Rowe and Hinchberger, 1998; Hinchberger and Rowe, 2005; Mabssout et al., 2006; Yin and Hicher, 2008). In order to determine the viscosity parameters, laboratory tests at very low loading rates are required. However, it is not an easy task to define how low the rate should be. According to the oedometer test results by Leroueil et al. (1985), the rate should be less than 10^{-8} s^{-1}. Unfortunately, these types of tests are not feasible to be conducted for geotechnical practice. Due to this reason, the conventional overstress models are not suitable for practical use. In order to overcome this limitation, the extended overstress models have been proposed.
(2) Extended overstress models, assuming viscoplastic strains occurring even though the stress state is inside of the static yield surface. In these models, it is not necessary to determining parameters using laboratory tests at very low loading rates. Instead, the determination for the initial size of static yield surface with parameters of soil viscosity is straightforward. Models fall into this category can be found in works by Adachi and Oka (1982), Kutter and Sathialingam (1992), Vermeer and Neher (1999), Yin et al. (2002) and Kimoto and Oka (2005). Among these investigators, Adachi and Oka's (1982) model is conventional overstress model, however, they stated that a pure elastic region is not necessarily used, thus, it can be included in this category.

The models by Vermeer and Neher (1999) and Yin et al. (2002) based on the concept of Bjerrum (1967) are also termed as creep

* Corresponding author. Address: Research Institute in Civil and Mechanical Engineering, GeM UMR CNRS 6183, Ecole Centrale de Nantes, BP 92101, 44321 Nantes Cédex 3, France. Tel.: +33 240371664; fax: +33 240372535.
E-mail addresses: zhenyu.yin@gmail.com (Z.-Y. Yin), chang@ecs.umass.edu (C.S. Chang), minna.karstunen@strath.ac.uk (M. Karstunen), pierre-yves.hicher@ec-nantes.fr (P.-Y. Hicher).

0020-7683/$ - see front matter © 2009 Elsevier Ltd. All rights reserved.
doi:10.1016/j.ijsolstr.2009.11.004

models in this paper. The creep models use secondary compression coefficient $C_{\alpha e}$ as input parameter for soil viscosity, which is easily obtained for engineering practice. However, the assumption used by Vermeer and Neher (1999) and Yin et al. (2002) on the flow direction of viscoplastic strain has some predicament. The assumption would have a consequence of predicting a strain-softening behaviour for undrained triaxial tests on isotropically consolidated samples and the stress path cannot overpass the critical state line for normally consolidated clay, which is not in agreement with experimental observations on slightly structured or reconstituted clays.

Recently, anisotropic models have been developed by Leoni et al. (2008) and Zhou et al. (2005) as extension of the isotropic creep models by Vermeer and Neher (1999), and Yin et al. (2002). However, in their models, the same assumption used by Vermeer and Neher (1999) and Yin et al. (2002) was kept. Therefore, the same problem mentioned above also appears in these models.

In the present paper, we propose a new model with three features:

(1) The elasto-viscoplastic overstress approach is adopted and extended in such a way that the parameters can be determined directly from either the constant strain-rate tests or the conventional creep tests, although the model is based on strain-rate rather than creep phenomenon.
(2) The new model does not have the same assumption on flow rule as that used in the creep models by Vermeer and Neher (1999) and Yin et al. (2002). Thus the new model can avoid the predictive limitations.
(3) The model is applicable to general inherent and induced anisotropic soil.

In the following, the limitations of existing models will first be discussed. The new model will then be proposed, which utilizes a strain-rate based scaling function and incorporates the extended overstress approach. The performance of this model will then be validated by the constant strain-rate (CRS) and creep tests under one-dimensional and triaxial conditions on St. Herblain clay.

2. Limitation of the existing models

2.1. Limitation of conventional overstress model

In a conventional overstress model, the material is assumed to behave elastically during the sudden application of a strain increment, which brings the stress state temporally beyond the yield surface. Then viscoplastic strain occurs. This will cause an expansion of yield surface due to strain hardening and simultaneously cause the stress relaxation due to the reduction of elastic strain.

Based on the conventional overstress model, the viscoplastic strain will not occur when the stress state is located within the static yield surface. However, the experimental results have indicated that the viscoplastic strain always occur, implying that the static yield surface never exists. Thus, the fundamental hypothesis of the conventional overstress model is in conflict with the experimental interpretation.

In order to look into this issue, we have examined the experimental results of CRS tests. The selected experimental tests were performed on clays of different mineral contents and Atterberg limits. Fig. 1 shows the classification of these clays using Casagrande's plasticity chart. According to this chart, the selected experimental results consist of low plastic, high plastic inorganic clays, and high plastic silty clays as indicated in Fig. 1.

Fig. 2 shows the schematic stress–strain–strain-rate behaviour of oedometer test on clays based on experimental observations (e.g., Graham et al., 1983; Leroueil et al., 1985, 1988; Nash et al., 1992; Rangeard, 2002). The apparent preconsolidation pressure

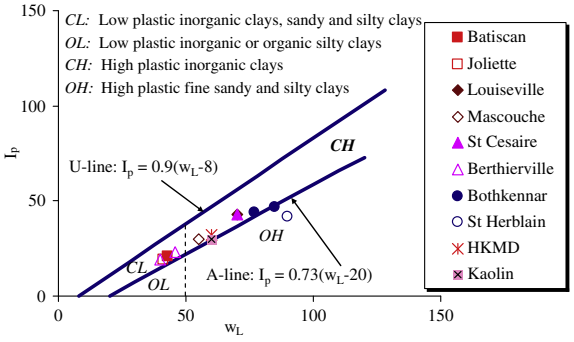

Fig. 1. Classification of soils by liquid limit and plasticity index.

σ'_p is dependent on the strain-rate. Fig. 3 shows linear relationships between the strain-rate and the apparent preconsolidation pressure in the double log plot of σ'_p/σ'_{v0}—$d\varepsilon_v/dt$ (preconsolidation pressure normalized by in situ vertical effective stress versus vertical strain-rate).

It is noted that for low strain-rate, the values of σ'_p can be smaller than their σ'_{v0}, even though the samples are under natural deposition for years, such as the Bäckebol and Berthierville clays.

Fig. 4 is a schematic plot in the double log plot of σ'_p—$d\varepsilon_v/dt$. This figure indicates different assumptions made by different models. For conventional overstress models by Shahrour and Meimon (1995), Fodil et al. (1997), Hinchberger and Rowe (2005) and Yin and Hicher (2008), a limiting initial static yield σ'_p was assumed at a very low strain-rate (point *C*), corresponding to the initial equilibrium state. Within the region of low strain-rate the path *A*–*C* is nonlinear. The viscosity parameters can be back-calculated from strain-rate test or 24 h standard oedometer test. The viscosity parameters strongly depend on the assumed value of the initial static yield stress σ'_p, which is somehow arbitrary. For the conventional overstress model by Rowe and Hinchberger (1998), an initial static yield stress σ'_p was assumed corresponding to a very low strain-rate (point B) below which the yield stress is constant. Within the region of low strain-rate the linear path *A*–*B* is followed by another linear path *B*–*C*. For the strain-rate smaller than B, the yield stress σ'_p does not change. Point *B* corresponds to the initial equilibrium state. Again, the viscosity parameters strongly depend on the assumed value of the initial static yield stress σ'_p.

In the conventional overstress model, the values of initial static yield stress σ'_p are generally assumed to be greater or equal to σ'_{v0}. However, the test results show otherwise as indicated in Fig. 4, in which the value of σ'_p can be smaller than σ'_{v0}, even for the samples under natural deposition for years. Thus, the value of initial static yield stress σ'_p for the conventional overstress model is difficult to be assumed.

This deficiency can be overcome by assuming the linear line extended indefinitely (see the path *A*–*D* as shown in Fig. 4). In this

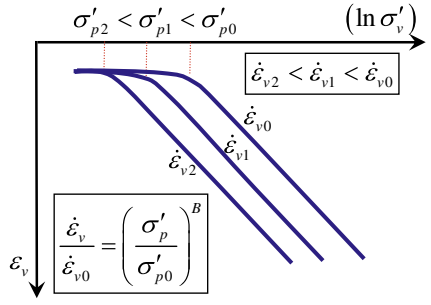

Fig. 2. Schematic plot of stress–strain–strain-rate behaviour of oedometer test.

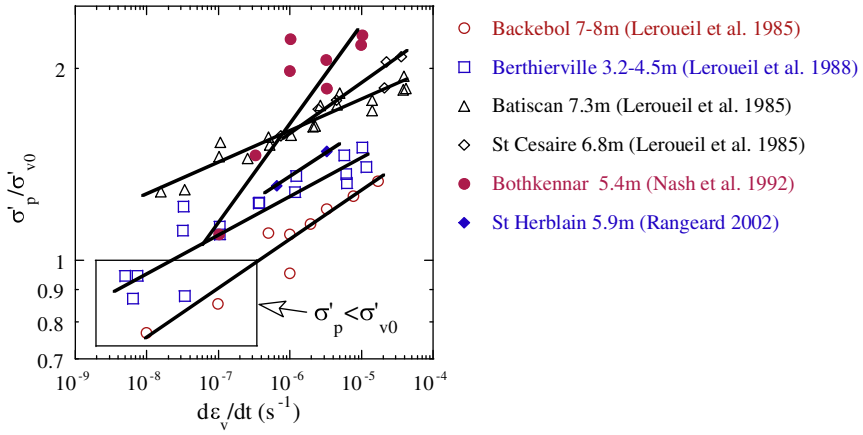

Fig. 3. Strain-rate effect on the apparent preconsolidation pressure for oedometer tests.

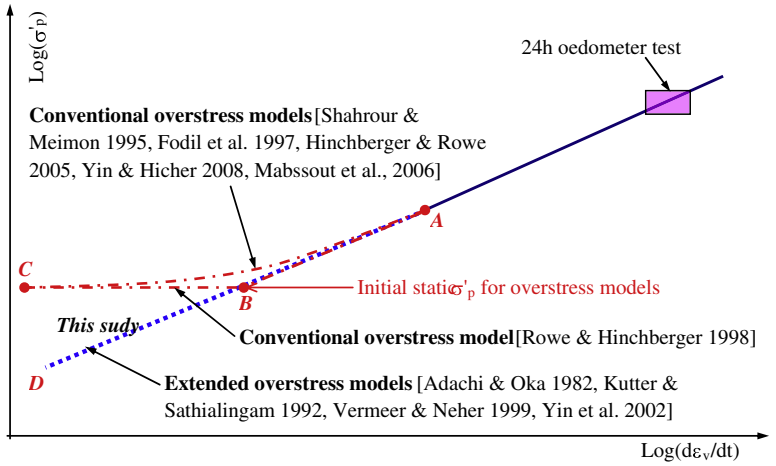

Fig. 4. Schematic plot for the relationship between the strain-rate and the apparent preconsolidation pressure by different assumptions of models.

way, the initial static yield stress does not exist. Therefore, there is no need to assume the initial value of static yield stress. The conventional overstress model is then extended and able to produce viscoplastic strains indefinitely in time. It also implies that viscoplastic strains may occur in elastic region.

However, it is to be noted that, until now, there is no experimental evidence about the relationship between σ'_p and $d\varepsilon_v/dt$ for very low strain-rate $d\varepsilon_v/dt < 1 \times 10^{-8}\ s^{-1}$. The lack of data are expected because it requires a very long duration for tests at low strain-rate (e.g., a test at $d\varepsilon_v/dt = 1 \times 10^{-9}\ s^{-1}$ for $\varepsilon_v = 10\%$ needs 3.2 years). Therefore, the linear relationship at very low strain level is only a hypothesis. There is no evidence to prove it one way or another.

However, if the linear hypothesis is made, the predicted viscoplastic phenomenon would be equivalent to that for creep models by Kutter and Sathialingam (1992), Vermeer and Neher (1999) and Yin et al. (2002). Thus, from a practical point of view, we adopt the linear hypothesis. Using this hypothesis, there is no need to assume a value of initial static yield stress. A value of reference σ'_p can be easily determined from an oedometer test at constant strain-rate, or from the standard conventional oedometer test which is the same as the method used in creep models.

2.2. Deficiency of creep models

Many clays exhibit strain-hardening behaviour under undrained triaxial compression. Fig. 5(a) shows the typical strain-hardening behaviour for an intact sample of slightly structured natural clay (St. Herblain clay by Zentar (1999)), a reconstituted sample of Hong Kong Marine Deposit (HKMD by Yin et al. (2002)), and an artificial pure clay sample (Kaolin by Biarez and Hicher (1994)). Fig. 5(b) shows the comparison between the experimental results and the simulation by the creep model by Yin et al. (2002). Although the model captured the undrained shear strength for the applied strain-rate, the predicted strain-softening behaviour is unrealistic compared to experimental one. Vermeer and Neher (1999) also showed the predicted strain-softening behaviour for undrained triaxial compression tests on isotropically consolidated samples by their proposed creep model. It is worth pointing out that the tests selected by Vermeer and Neher (1999) were conducted on samples of intact Haney clay (Vaid and Campanella, 1977) which is a structured clay with sensitivity $s_t = 6$–10. Thus the experimental strain-softening behaviour is due to the degradation of bonds during the shearing.

During the step-changed undrained triaxial tests at constant strain-rate, the stress path can overpasses the critical state line during the loading with the strain-rate higher than the strain-rate at previous loading stage. Fig. 6 shows the normalized effective stress paths for HKMD by Yin and Cheng (2006). C150 and C400 are the tests under a confining pressure of 150 kPa and 400 kPa, respectively. The critical state line was estimated using three undrained triaxial tests at one constant strain-rate (see Yin and Cheng, 2006). In these two step-changed tests, stress path overpasses the critical

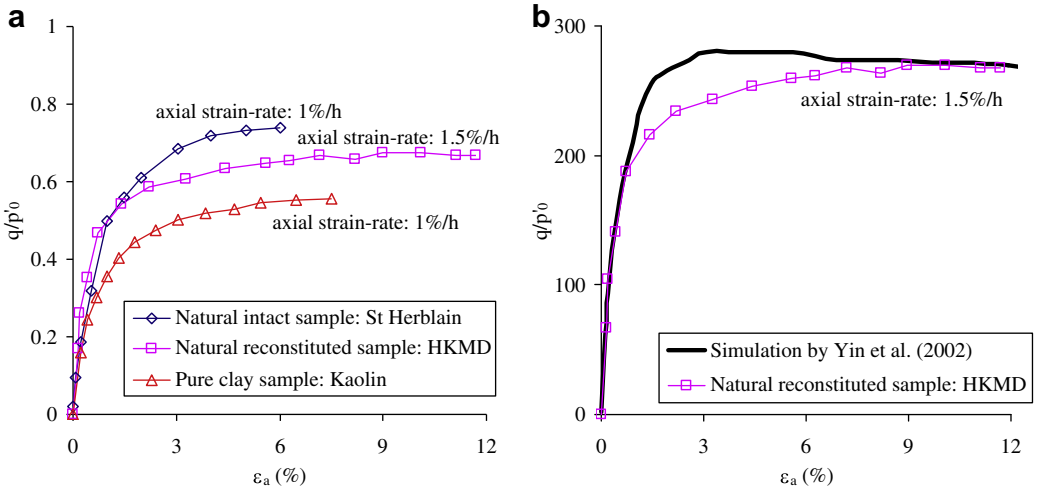

Fig. 5. (a) Strain-hardening behaviour of clays, and (b) predicted strain-softening behaviour by Yin et al. (2002).

state line during the loading stage at a high strain-rate of 20%/h, which follows the loading stage at a low strain-rate of 0.2%/h.

The behaviour that the stress path overpasses the critical state line in a step-changed undrained triaxial test cannot be predicted using the creep models by Vermeer and Neher (1999) and Yin et al. (2002). This deficiency of creep models is a consequence of the bad assumption on the viscoplastic volumetric strain-rate $d\varepsilon_v^{vp}/dt$, which is assumed independent of the stress state. This assumption results in an unreasonably large value of viscoplastic volumetric strain as the stress state approaches the critical state line, while the value should be nearly zero based on the experimental observations. Due to the unduly large volume contraction, instability occurs and the models start to predict strain-softening behaviour as shown in the predicted curves of q–ε_a (deviatoric stress versus axial strain) for undrained triaxial tests on isotropically consolidated samples by Vermeer and Neher (1999) and Yin et al. (2002).

The anisotropic models by Zhou et al. (2005) and Leoni et al. (2008) utilize the same assumption on viscoplastic volumetric strain-rate, thus these two models also have the same deficiencies.

2.3. Need for a general anisotropic model

Another fundamental feature of soft clay concerns anisotropy, as the stress–strain behaviour of soft clay is stress-dependent, and a significant degree of anisotropy can be developed during their deposition, sedimentation, consolidation history and any subsequent straining. This has been experimentally and numerically investigated at the scale of specimen (see, e.g., Tavenas and Leroueil, 1977; Burland, 1990; Diaz Rodriguez et al., 1992; Wheeler et al., 2003; Karstunen and Koskinen, 2008) and at the microstructure scale (see, e.g., Hicher et al., 2000; Yin et al., 2009). The anisotropy affects the stress–strain behaviour of soils, and therefore needs to be taken into account. Isotropic conventional and extended overstress models may work reasonably well for reconstituted soils under fixed loading conditions. As indicated by Leoni et al. (2008), it is necessary to incorporate anisotropy while predicting the stress–strain-time behaviour of soft natural soils. However, very few anisotropic models exist for strain-rate analyses. The anisotropic models by Zhou et al. (2005) and Leoni et al. (2008) have deficiencies as mentioned in last section. In the anisotropic models by Adachi and Oka (1982) and Kimoto and Oka (2005), the yield surface does not rotate with applied stresses, thus the models have neglected the stress induced anisotropy. The elasto-viscoplastic model by Oka (1992) and the viscoelastic–viscoplastic model by Oka et al. (2004) extended from the model of Adachi and Oka (1982) have incorporated a kinematic hardening law for the rotation of yield surfaces requiring three additional parameters being determined by curve fitting.

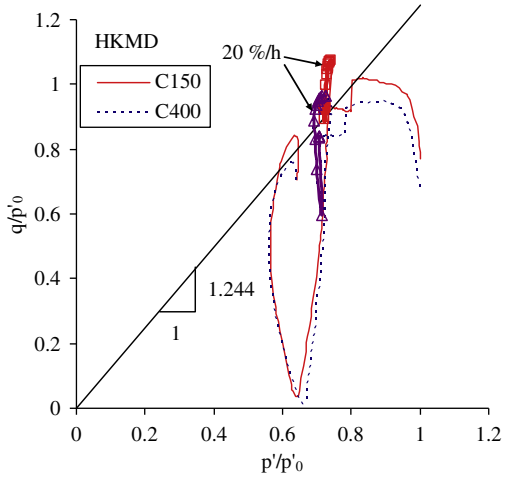

Fig. 6. Stress path overpass the critical state line for normally consolidated clay.

3. Proposed constitutive model

A new model will be presented here that has the following three features: (1) it is a general anisotropic model, (2) it overcomes the limitation of conventional overstress models, and (3) it overcomes the deficiency of creep models.

3.1. Modification on overstress formulation

The proposed time-dependent approach was extended from the overstress theory by Perzyna (1963, 1966). In order to take into account soil anisotropy, an inclined elliptical yield surface was adopted with a rotational hardening law proposed by Wheeler et al. (2003).

According to Perzyna's overstress theory (1963, 1966), the total strain-rate is additively composed of the elastic strain-rates and viscoplastic strain-rates. The elastic behaviour in the proposed model is assumed to be isotropic. The viscoplastic strain-rate $\dot{\varepsilon}_{ij}^{vp}$

is assumed to obey an associated flow rule with respect to the dynamic loading surface f_d (Perzyna, 1963, 1966):

$$\dot{\varepsilon}_{ij}^{vp} = \mu\langle\Phi(F)\rangle\frac{\partial f_d}{\partial\sigma'_{ij}} \tag{1}$$

where the symbol $\langle\ \rangle$ is defined as $\langle\Phi(F)\rangle = \Phi(F)$ for $F > 0$ and $\langle\Phi(F)\rangle = 0$ for $F \leqslant 0$. μ is referred to as the fluidity parameter; the dynamic loading surface f_d is treated as a viscoplastic potential function; $\Phi(F)$ is the overstress function representing the distance between the dynamic loading surface and the static yield surface. When the equilibrium state is reached, or stress state is within the static yield surface ($F \leqslant 0$), the rate of viscoplastic volumetric strain is zero.

A power-type scaling function based on the strain-rate oedometer tests was adopted for the viscoplastic strain-rate:

$$\Phi(F) = \left(\frac{F_d}{F_s}\right)^N \tag{2}$$

where N is the strain-rate coefficient. F_d/F_s is a measure representing the overstress caused by the distance between the dynamic loading surface and the static yield surface. Adachi and Oka (1982) replaced the ratio F_d/F_s by a ratio of the size of dynamic loading surface p_m^d to that of static yield surface p_m^s (i.e., p_m^d/p_m^s). This is different from the method of using parallel yield surface tangents (i.e., $1 + \sigma_{os}'^d/p_m^s$ see Fig. 7(a)) proposed by Rowe and Hinchberger (1998). By using p_m^d/p_m^s, it greatly simplifies the process of calibrating viscosity parameters.

In the present model (see Fig. 7(b)), Perzyna's overstress theory in Eq. (1) is modified by

$$\dot{\varepsilon}_{ij}^{vp} = \mu\left\langle\left(\frac{p_m^d}{p_m^r}\right)^N\right\rangle\frac{\partial f_d}{\partial\sigma'_{ij}} \tag{3}$$

In this equation, the rate of viscoplastic volumetric strain always exists, even for the ratio p_m^d/p_m^r less than one. Instead of static yield surface, we term the initial surface as a reference surface (with a reference size p_m^r), which refers to the value of apparent preconsolidation stress obtained from a selected experimental test. Since there is no restriction for the occurrence of viscoplastic strain, it implies that viscoplastic strain can occur in an elastic region.

Due to the elliptic-shaped yield surface adopted in this new model, as shown in Fig. 7(b), the relationship $OA/OB = \sigma'_{ij}/\sigma'^{rr}_{ij} = p'/p'_r = q/q_r = p_m^d/p_m^r$ can be obtained for an arbitrary constant stress ratio η. Thus, for the case of K_{nc}-consolidation, the relationship between the apparent preconsolidation pressure and the size of surfaces is given by $\sigma'_p/\sigma'^r_p = p_m^d/p_m^r$.

The proposed formulation therefore implies a linear relationship between $\log(\dot{\varepsilon}_v^{vp})$ and $\log\left(\sigma'_p\right)$, which agrees with the experimental evidence shown in Fig. 3.

3.2. A general anisotropic strain-rate model

In this model, an elliptical surface is adopted to describe the dynamic loading surface and the reference surface. The elliptical function of dynamic loading surface, following the ideas by Wheeler et al. (2003), is rewritten in a general stress space as:

$$f_d = \frac{\frac{3}{2}(\sigma'_d - p'\alpha_d) : (\sigma'_d - p'\alpha_d)}{\left(M^2 - \frac{3}{2}\alpha_d : \alpha_d\right)p'} + p' - p_m^d = 0 \tag{4}$$

where σ'_d is the deviatoric stress tensor; α_d is the deviatoric fabric tensor, which is dimensionless but has the same form as deviatoric stress tensor (see Appendix A); M is the slope of the critical state line; p' is the means effective stress; and p_m^d is the size of dynamic loading surface corresponding to the current stress state. For the special case of a cross-anisotropic sample, the scalar parameter $\alpha = \sqrt{3/2(\alpha_d : \alpha_d)}$ defines the inclination of the ellipse of the yield curve in q–p' plane as illustrated in Fig. 7.

The reference surface has an elliptical shape identical to the dynamic loading surface (see Eq. (4)), but has a different size p_m^r.

To interpolate M between its values M_c (for compression) and M_e (for extension) by means of the Lode angle θ (see Sheng et al., 2000), which reads as:

$$M = M_c\left[\frac{2c^4}{1 + c^4 + (1 - c^4)\sin 3\theta}\right]^{\frac{1}{4}} \tag{5}$$

where $c = \frac{M_e}{M_c}$, $\frac{-\pi}{6} \leqslant \theta = \frac{1}{3}\sin^{-1}\left(\frac{-3\sqrt{3}\bar{J}_3}{2\bar{J}_2^{3/2}}\right) \leqslant \frac{\pi}{6}$ with $\bar{J}_2 = \frac{1}{2}\bar{s}_{ij} : \bar{s}_{ij}$ and $\bar{J}_3 = \frac{1}{3}\bar{s}_{ij}\bar{s}_{jk}\bar{s}_{ki}$, and $\bar{s}_{ij} = \sigma_d - p'\alpha_d$.

The expansion of the reference surface, which represents the hardening of the material, is assumed to be due to the inelastic volumetric strain ε_v^{vp}, similarly to the critical state models:

$$dp_m^r = p_m^r\left(\frac{1 + e_0}{\lambda - \kappa}\right)d\varepsilon_v^{vp} \tag{6}$$

where λ is the slope of the normal compression curve in the e–$\ln\sigma'_v$, κ is the slopes of the swelling-line and e_0 is the initial void ratio.

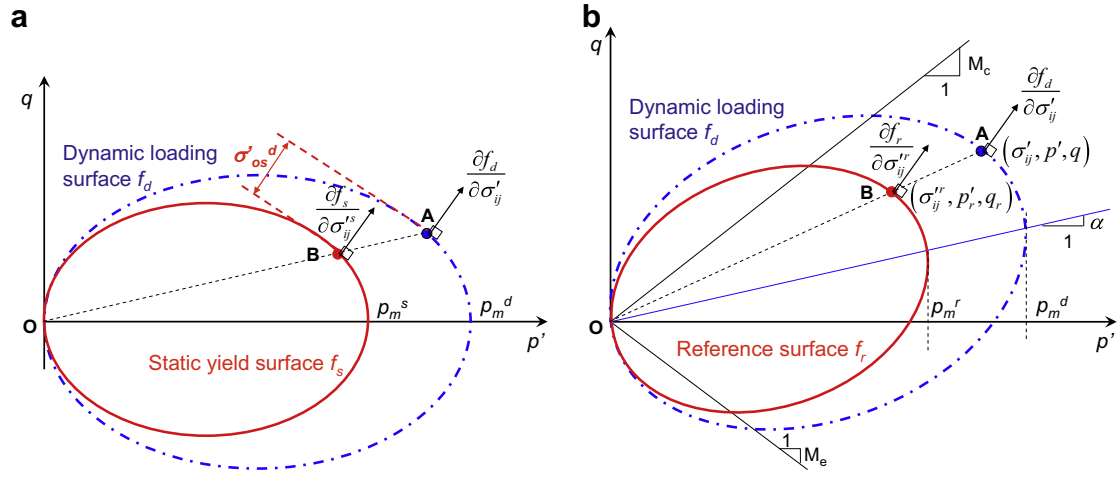

Fig. 7. Definition of overstress model in p'–q space.

The rotational hardening law, based on the formulation proposed by Wheeler et al. (2003), describes the development of anisotropy caused by viscoplastic strains. Both volumetric and deviatoric viscoplastic strains control the rotation of the yield curve.

$$d\alpha_d = \omega\left[\left(\frac{3\sigma_d}{4p'} - \alpha_d\right)\left\langle d\varepsilon_v^{vp}\right\rangle + \omega_d\left(\frac{\sigma_d}{3p'} - \alpha_d\right)d\varepsilon_d^{vp}\right] \tag{7}$$

where the function of MacCauley is $\langle d\varepsilon_v^{vp}\rangle = (d\varepsilon_v^{vp} + |d\varepsilon_v^{vp}|)/2$. The soil constant ω controls the rate at which the deviatoric fabric tensor heads toward their current target values, and ω_d controls the relative effect of viscoplastic deviatoric strains on the rotation of the elliptical surface.

The proposed model was implemented as a user-defined model in the 2D Version 8 of PLAXIS using the numerical solution proposed by Katona (1984). The basic finite element scheme for the proposed model is similar to the ones presented by Oka et al. (1986) and Rowe and Hinchberger (1998). For a coupled consolidation analysis based on Biot's theory, the relationship of the load increment is given by applying the principle of virtual work to the equilibrium equation as shown by Oka et al. (1986). The coupled finite element equations are well documented by several researchers (e.g., Oka et al., 1986; Britto and Gunn, 1987; Rowe and Hinchberger, 1998), and not repeated here.

3.3. Correction for deficiency of creep models

For the creep models by Vermeer and Neher (1999) and by Yin et al. (2002), the viscous volumetric strain-rate is obtained from the secondary compression coefficient $C_{\alpha e}$ defined in e-ln$t$ space, given by Eqs. (8a) and (8b), respectively

$$\dot{\varepsilon}_v^{vp} = \frac{C_{\alpha e}}{(1+e_0)\tau}\left(\frac{p'_c}{p'_{c0}}\right)^{\frac{\lambda-\kappa}{C_{\alpha e}}} \tag{8a}$$

$$\dot{\varepsilon}_v^{vp} = \frac{C_{\alpha e}}{(1+e_0)\tau}\left(1+\frac{d\varepsilon_v}{\varepsilon_{vl}^{vp}}\right)^2 \exp\left[\frac{d\varepsilon_v}{\left(1+\frac{d\varepsilon_v}{\varepsilon_{vl}^{vp}}\right)}\frac{(1+e_0)}{C_{\alpha e}}\right] \tag{8b}$$

where τ is the reference time; p'_c is the size of the potential surface corresponding to the current stress state; p'_{c0} is the size of the reference surface; ε_{vl}^{vp} is the limit of viscoplastic volumetric strain.

The deviatoric component of stain-rate is obtained from the volumetric strain-rate by a flow rule. In this formulation, the volumetric strain-rate is not a function of η. However, experimental evidence has shown that the volumetric strain-rate is nearly zero when η approaches the critical state line. Therefore, this equation would result an unrealistically large volume strain-rate when η is near critical state line.

In the present model, the strain-rate is obtained from the potential function f_d as shown in Eq. (3), which has the same form as the elliptical yield surface proposed by Wheeler et al. (2003). Thus in the present model, the volumetric strain-rate is dependent on the value η and the volumetric strain-rate approaches zero as the η approaches the critical state line. This would avoid the deficiencies of creep models as will be shown in the model validation.

4. Summary of model parameters

The proposed model involves a number of soil parameters and state parameters which can be divided into three main groups:

(1) The first set of parameters which are similar to the Modified Cam Clay parameters (Roscoe and Burland, 1968) include Poisson's ratio (υ'), slope of the compression line (λ), slope of the swelling-recompression line (κ), initial void ratio (e_0), stress ratio at critical state in compression and extension (M_c, M_e) and the initial reference preconsolidation pressure $\left(\sigma_{p0}^{rr}\right)$.
(2) The second set relates to the initial anisotropy α and relates to the rotation rate of dynamic loading and reference surfaces ω.
(3) The third set relates to viscosity (N, μ).

The required model parameters are listed in Table 1.

4.1. Modified Cam Clay parameters

The Modified Cam Clay parameters include Poisson's ratio (υ'), slope of the compression line (λ), slope of the swelling-recompression line (κ), initial void ratio (e_0), stress ratio at critical state in compression and extension (M_c, M_e) and the size of the initial reference surface (p'_{m0}). All seven parameters can be determined in a standard process from triaxial and oedometer tests.

The initial reference preconsolidation pressure σ_{p0}^{rr} obtained from oedometer test is used as an input to calculate the initial size p'_{m0} by the following equation (derived from Eq. (4) of reference surface):

Table 1
State parameters and soil constants of natural soft clay creep model.

Group	Parameter	Definition	Determination	St. Herblain	
				Based on CRS test	Based on 24 h test
Standard model parameters	σ_{p0}^{rr}	Initial reference preconsolidation pressure	From oedometer test	52 kPa	39 kPa
	e_0	Initial void ratio (state parameter)	From oedometer test	2.19	2.26
	υ'	Poisson's ratio	From initial part of stress–strain curve (typically 0.15–0.35)	0.2	0.2
	κ	Slope of the swelling line	From ID or isotropic consolidation test	0.022	0.038
	λ	Slope of the compression line	From ID or isotropic consolidation test	0.4	0.48
	$M_c(M_e)$	Slope of the critical state line	From triaxial shear test (M_c for compression and M_e for extension)	1.2(1.05)	1.2(1.05)
Anisotropy parameters	α_0	Initial anisotropy (state parameter for calculating initial components of the fabric tensor)	For K_0-consolidated samples $\alpha_0 = \alpha_{K0} = \eta_{K0} - \frac{M_c^2 - \eta_{K0}^2}{3}$	0.48	0.48
	ω	Absolute rate of yield surface rotation	$\omega = \frac{1+e_0}{(\lambda-\kappa)\ln R}\ln\frac{M^2\alpha_{K0}/\alpha - 2\alpha_{K0}\omega_d}{M^2 - 2\alpha_{K0}\omega_d}$ or from undrained triaxial extension test	80	80
Viscosity parameters	μ	Fluidity	From conventional oedometer test or oedometer test at constant strain-rates	8.7×10^{-7} s^{-1}	7.4×10^{-8} s^{-1}
	N	Strain-rate coefficient		11.2	12.9

$$p'_{m0}=\left\{\frac{[3-3K_0-\alpha_{K0}(1+2K_0)]^2}{3\left(M_c^2-\alpha_{K0}^2\right)(1+2K_0)}+\frac{(1+2K_0)}{3}\right\}\sigma'^{r}_{p0} \tag{9}$$

where K_0 is the coefficient of earth pressure at rest, which can be calculated from the critical state parameter M_c by Jaky's formula; α_{K0} is the initial anisotropy of natural undisturbed sample, which can also be calculated from M_c (Wheeler et al., 2003):

$$K_0=\frac{6-2M_c}{6+M_c} \tag{10}$$

$$\alpha_{K0}=\eta_{K0}-\frac{M_c^2-\eta_{K0}^2}{3}\quad\text{with}\quad\eta_{K0}=\frac{3M_c}{6-M_c} \tag{11}$$

4.2. Parameters of anisotropy

The initial anisotropy α_0 depends on the deposition history of soils. For natural soils and reconstituted soils which are commonly sedimented under K_0-consolidation, $\alpha_0=\alpha_{K0}$. can be determined from Eq. (11) The value for the soil constant ω_d can be determined from the critical state parameter M_c as proposed by Wheeler et al. (2003):

$$\omega_d=\frac{3\left(4M_c^2-4\eta_{K0}^2-3\eta_{K0}\right)}{8\left(\eta_{K0}^2+2\eta_{K0}-M_c^2\right)} \tag{12}$$

When the soil is subjected to an isotropic loading, the inclination of surfaces will be reduced from an initial value α_{K0} to α. The amount of this reduction depends on the rotation rate constant ω. The parameter ω can be derived from Eq. (7) by integrating the differential equation and considering isotropic loading, as shown by Leoni et al. (2008). The general formulation for ω is given by:

$$\omega=\frac{1+e_0}{(\lambda-\kappa)\ln R}\ln\frac{M_c^2\alpha_{K0}/\alpha-2\alpha_{K0}\omega_d}{M_c^2-2\alpha_{K0}\omega_d} \tag{13}$$

where R is the ratio p'_f/p'_{p0} as shown in Fig. 8 where p'_f is the final stress of the isotropic consolidation stage and p'_{p0} is the preconsolidation pressure obtained from this isotropic consolidation stage. The value α is the new inclination due to the isotropic consolidation up to p'_f. Leoni et al. (2008) used $\alpha_{K0}/\alpha=10$ for the case $\ln R=1$ to calculate ω based on the suggestion by Anandarajah et al. (1996)

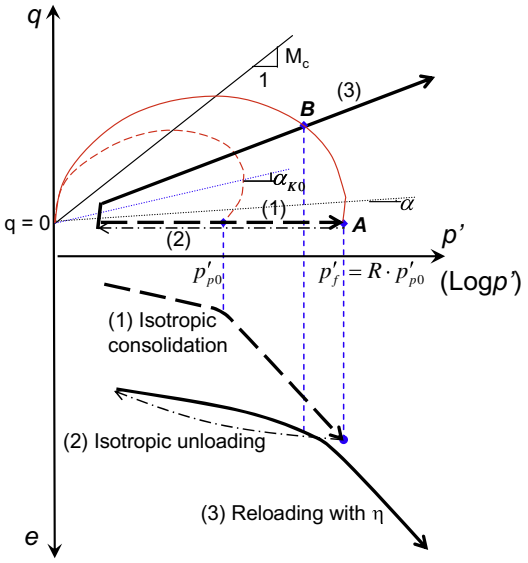

Fig. 8. Step-changed consolidation test to determine the anisotropic parameter ω.

for Kaolinite. However, $\alpha_{K0}/\alpha=10$ is not always true for other types of clay, and Leoni et al. (2008) did not propose an experimental method to determine the value of α. In order to determine α, one possible way is to carry out a step-changed drained triaxial test, as shown in Fig. 8. This test consists of three stages: an isotropic consolidation (path 1), isotropic unloading (path 2), and followed by a reloading with $\eta\neq 0$ (path 3). The isotropic loading is used to determine $R=p'_f/p'_{p0}$. From reloading stage the yield stress point B can be determined (see Fig. 8). The new apparent yield surface passing through points A and B can be used to estimate α by Eq. (14), which is simplified from Eq. (4) for p'–q space (A is the final state of isotropic consolidation).

$$(q-p'\alpha)^2+(M^2-\alpha^2)(p'-p'^{d}_m)p'=0 \tag{14}$$

Once the α is estimated, the ω can be calculated by Eq. (13).

This step-changed test mentioned above can also be a consolidation stage of triaxial shear test for determining M. Therefore, no additional test is needed, compared to the Modified Cam Clay model.

4.3. Parameters related to viscosity

The viscous parameters μ and N in the present model (see Eq. (3)) can be determined either from: (1) an oedometer test at constant strain-rates (CRS) or (2) a conventional oedometer test. The process will be discussed in this section.

(1) *Determine parameters from a constant strain-rate oedometer test*

In the proposed model, the flow rule in Eq. (3) is determined from the dynamic loading surface of Eq. (4). Under a triaxial stress condition, the viscoplastic volumetric strain-rate can be derived as:

$$\dot{\varepsilon}_v^{vp}=\mu\left(\frac{p_m^d}{p_m^r}\right)^N\frac{M^2-\eta^2}{M^2-\alpha^2} \tag{15}$$

For the special case of one-dimensional compression, $\eta=\eta_{K0}$ and $\alpha=\alpha_{K0}$. Using the relationship $\sigma'_p/\sigma'^{r}_p=p_m^d/p_m^r$ (see Fig. 7), Eq. (15) becomes

$$\dot{\varepsilon}_v^{vp}=\mu\left(\frac{\sigma'_p}{\sigma'_{p0}}\right)^N\frac{M_c^2-\eta_{k0}^2}{M_c^2-\alpha_{k0}^2} \tag{16}$$

As shown in Figs. 2 and 3, the linear relationship in the double log plot of σ'_p/σ'_{v0}–$\mathrm{d}\varepsilon_v/\mathrm{d}t$ is assumed in this proposed model:

$$\dot{\varepsilon}_v=A\left(\frac{\sigma'_p}{\sigma'_{p0}}\right)^B \tag{17}$$

The experimentally measured two parameters are A and B. The value B is the slope of σ'_p (or σ'_p/σ'_{v0})–$\mathrm{d}\varepsilon_v/\mathrm{d}t$ in double log space; σ'_{p0} is the reference preconsolidation pressure corresponding to the constant A (i.e., a reference strain-rate $\dot{\varepsilon}_{v0}$). From the definition of elastic and viscoplastic strains, the ratio between the elastic strain-rate and the viscoplastic strain-rate can be derived as:

$$\left.\begin{aligned}\varepsilon_v^e&=\tfrac{\kappa}{1+e_0}\ln\tfrac{\sigma'_v}{\sigma'_{v1}}\Rightarrow\dot{\varepsilon}_v^e=\tfrac{\kappa}{1+e_0}\tfrac{\dot{\sigma}'_v}{\sigma'_v}\\ \varepsilon_v^{vp}&=\tfrac{\lambda-\kappa}{1+e_0}\ln\tfrac{\sigma'_v}{\sigma'_{v1}}\Rightarrow\dot{\varepsilon}_v^{vp}=\tfrac{\lambda-\kappa}{1+e_0}\tfrac{\dot{\sigma}'_v}{\sigma'_v}\end{aligned}\right\}\Rightarrow\frac{\dot{\varepsilon}_v^e}{\dot{\varepsilon}_v^{vp}}=\frac{\kappa}{\lambda-\kappa} \tag{18}$$

The total strain-rate can then be written as:

$$\dot{\varepsilon}_v=\dot{\varepsilon}_v^e+\dot{\varepsilon}_v^{vp}=\frac{\lambda}{\lambda-\kappa}\dot{\varepsilon}_v^{vp} \tag{19}$$

Substituting Eq. (19) into Eq. (17), the viscoplastic volumetric strain can then be written as

$$\dot{\varepsilon}_v^{vp}=A\frac{\lambda-\kappa}{\kappa}\left(\frac{\sigma'_p}{\sigma'_{p0}}\right)^B \tag{20}$$

Comparing Eqs. (16) and (20), viscosity parameters can be obtained as follows:

$$\mu = \frac{A(\lambda-\kappa)}{\lambda}\frac{\left(M_c^2-\alpha_{K0}^2\right)}{\left(M_c^2-\eta_{K0}^2\right)} \quad \text{and} \quad N = B \tag{21}$$

where A and B are measured from the constant strain-rate tests as shown in Fig. 3.

(2) *Determine parameters from a conventional oedometer test*

Experimental evidence has shown that in a conventional oedometer test, soil creeps continuously under a constant load. The void ratio change versus log scale of time is a linear line with slope $C_{\alpha e}$. This is the basic underpinning for creep models. It is to be noted that, although creep models are based on the creep phenomenon of soils, the linear relationship between σ'_p/σ'_{v0}—$\mathrm{d}\varepsilon_v/\mathrm{d}t$ is also revealed (Kutter and Sathialingam, 1992; Vermeer and Neher, 1999) based on Bjerrum's concept of delayed compression.

Assuming the conventional oedometer test is performed with a duration t for each load increment, and a preconsolidation σ'_{p0} is measured from the test results, Kutter and Sathialingam (1992) and Vermeer and Neher (1999) suggested the following relationship:

$$\dot{\varepsilon}_v^{vp} = \frac{C_{\alpha e}}{(1+e_0)\tau}\left(\frac{\sigma'_p}{\sigma'_{p0}}\right)^{\frac{\lambda-\kappa}{C_{\alpha e}}} \tag{22}$$

Leoni et al. (2008) suggested that the reference time τ can be assigned equal to the duration of each load increment t for normally consolidated clay.

Compared this equation with the linear equation obtained from constant strain-rate tests (Eq. (20)), it follows:

$$A = \frac{\lambda}{(\lambda-\kappa)}\frac{C_{\alpha e}}{(1+e_0)\tau} \quad \text{and} \quad B = \frac{\lambda-\kappa}{C_{\alpha e}} \tag{23}$$

In connection to the present model, the viscosity parameters can be obtained as follows:

$$\mu = \frac{C_{\alpha e}\left(M_c^2-\alpha_{K0}^2\right)}{\tau_r(1+e_0)\left(M_c^2-\eta_{K0}^2\right)} \quad \text{and} \quad N = \frac{\lambda-\kappa}{C_{\alpha e}} \tag{24}$$

The reference time τ_r depends on the duration of incremental loading used in the conventional oedometer test, from which the initial reference preconsolidation pressure σ'^{r}_{p0} is obtained. A common duration used for the conventional oedometer test is 24 h.

5. Experimental results used for model validation

Experimental results obtained from St. Herblain clay is used here for model validation. St. Herblain clay is a river clayey alluvial deposit from the Loire Palaeolithic period, characterized as a slightly organic and high plastic clay with Plastic Limit w_P = 48% and Liquid Limit w_L = 90%. A shear strength profile measured from field vane tests is shown in Fig. 9. The specimens used for laboratory experiments were chosen from a depth of 4–8 m corresponding to a soft compressible clay layer with relatively homogeneous characteristics, estimated from the profile of field vane shear strength.

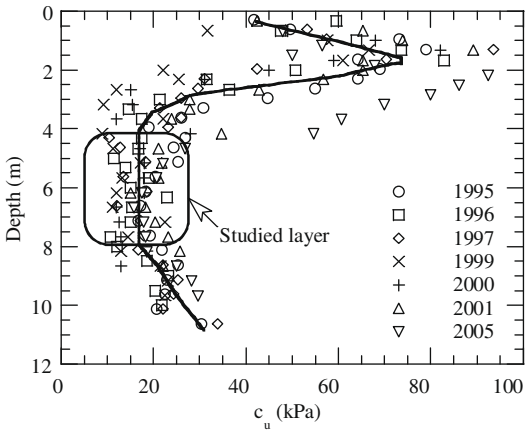

Fig. 9. Field vane test profiles for St. Herblain clay (after Zentar, 1999; Rangeard, 2002; Yin and Cheng, 2006).

Fig. 10 shows the photos of scanning electronic microscope of St. Herblain clay for horizontal and vertical directions of intact sample, and for reconstituted sample. The cluster size of horizontal direction looks bigger than that of vertical direction, which indicates that the long axis of the elliptical cluster is aligned horizontal due to its deposition history. Compared to the photo of reconstituted sample, the arrangement of clusters of natural clay sample is more anisotropic.

Zentar (1999) conducted drained triaxial tests under different stress paths to describe the apparent yield envelope as shown in Fig. 11. The axial strain-rate for all tests varies from 0.1×10^{-7} to $16.6 \times 10^{-7}\ \mathrm{s}^{-1}$, and volumetric strain-rate varies from 1.8×10^{-7} to $21 \times 10^{-7}\ \mathrm{s}^{-1}$. To determine an apparent yield curve from these measured yield points is difficult, since these yield points were obtained from tests of different strain-rates. An approximately inclined elliptical surface can be concluded, which experimentally supports the adopted surface shape of the model.

Besides the types of tests conducted on St. Herblain clay by Zentar (1999) and Rangeard (2002), we performed additional creep tests (i.e., a conventional oedometer test and an undrained triaxial creep test) on the same clay for this study. The database includes 24 h standard oedometer tests, oedometer tests at constant strain-rate with the measurement of lateral stress, undrained triaxial tests at constant strain-rate, and undrained triaxial creep tests. All test results, summarized in Table 2, were used for the experimental verification of the proposed model.

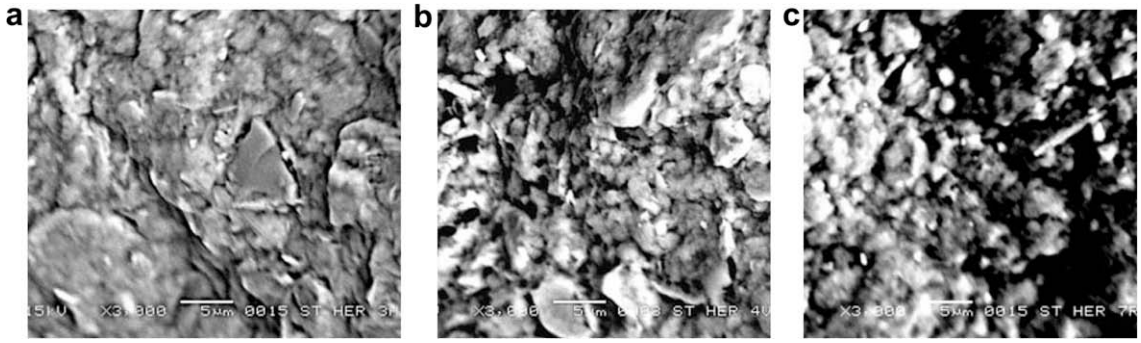

Fig. 10. SEM (scanning electron microscope) photos of St. Herblain clay for (a) horizontal direction, (b) vertical direction of intact sample, and (c) for reconstituted sample.

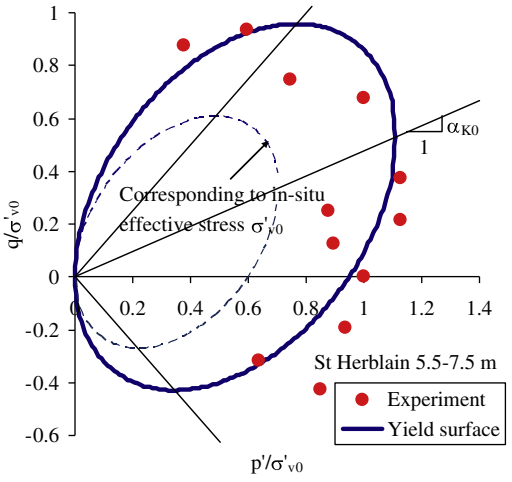

Fig. 11. Apparent yield curve of St. Herblain clay (after Zentar, 1999).

6. Model performance

In order to evaluate the model predictive ability, tests with different loading conditions were simulated. The calibration of model parameters was based on oedometer tests combined with undrained triaxial tests. Both CRS and 24 h oedometer tests were used separately to calibrate two sets of model parameters. Furthermore, simulations were made by switching the anisotropic features on and off, to explore the relative importance of anisotropy:

- For the case referred "Isotropic model", soil is assumed to be isotropic and only viscosity is considered (with $\alpha_0 = 0$ and $\omega = 0$).
- For the case referred "Anisotropic model", both anisotropy and viscosity are incorporated.

Table 2
Physical and mechanical characteristics of St. Herblain clay samples.

Test	Depth (m)	w (%)	e_i	γ (kN/m^3)	Description
Triaxial at constant strain-rate	5.5–6.5	89	2.32	14.76	Step-changed strain-rate
Triaxial creep	5.5–6.5	86	2.84	14.87	Step-changed stress level
Oedometer at constant strain-rate	6.9–6.95	87	2.26	14.85	Step-changed strain-rate
Oedometer consolidation	5.7–5.75	93	2.41	14.88	24 h standard consolidation

6.1. Calibration of model parameters

Two sets of parameters were determined: one from constant rate of strain tests and the other from 24 h conventional oedometer tests.

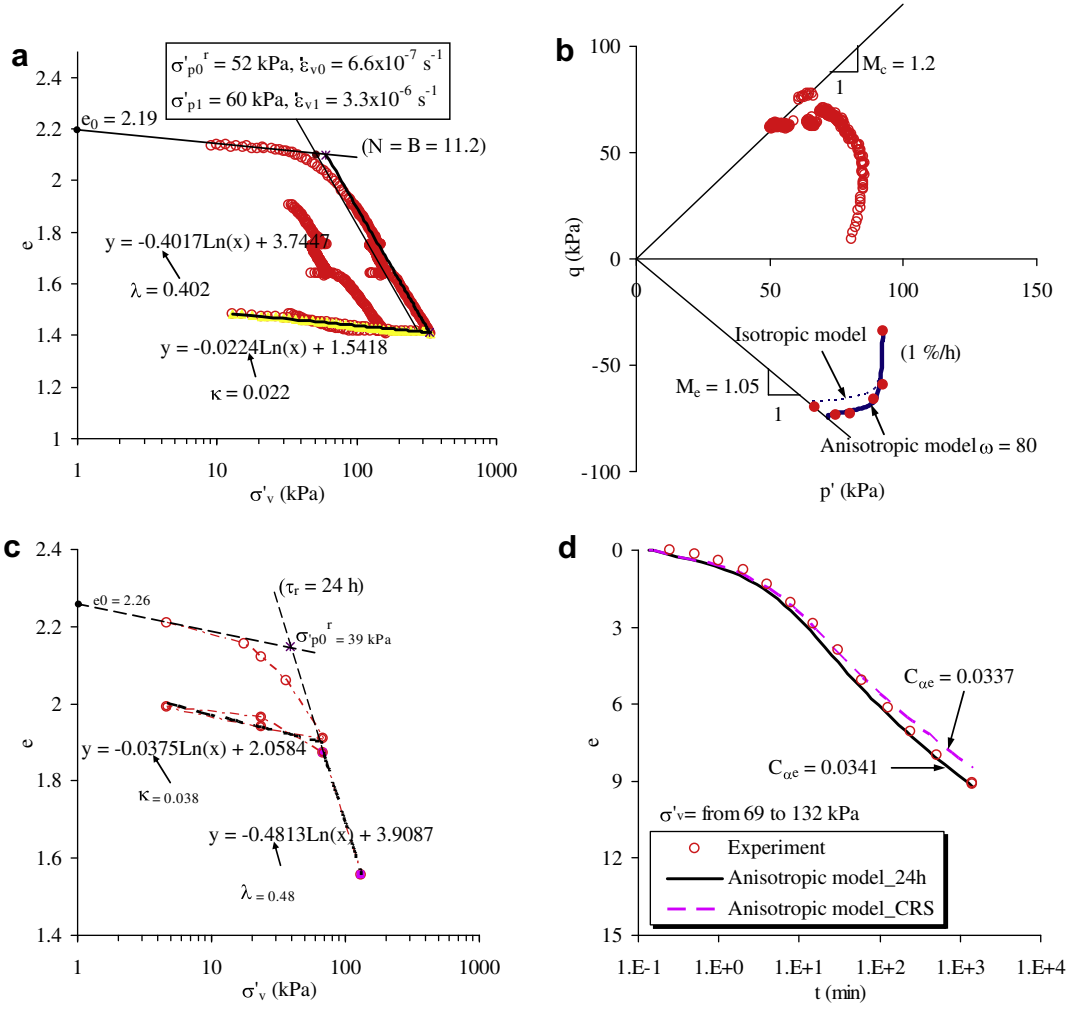

Fig. 12. Laboratory tests for calibrating model parameters: (a) oedometer test at constant strain-rates, (b) undrained triaxial tests in compression and extension, (c) 24 h conventional oedometer test, and (d) curve of settlement by time of oedometer test.

(1) *Determined from CRS oedometer tests*

The CRS test was conducted with multistage at two constant strain-rates ($\dot{\varepsilon}_v$) by using an oedometric cell providing measurements of horizontal stress in addition to vertical stress by Rangeard (2002). The test was performed at $\dot{\varepsilon}_v = 3.3 \times 10^{-6}$ s^{-1} until ε_v reaching at 12%, then changed to $\dot{\varepsilon}_v = 6.6 \times 10^{-7}$ s^{-1} until a vertical strain of 15.5%, and finally changed back to the initial strain-rate. The clay sample is from a depth of 6.9 m (see Fig. 12(a)).

The values for parameters λ, κ and e_0 were measured from CRS test (see Fig. 12(a)). The strain-rate $\dot{\varepsilon}_{v0} = 6.6 \times 10^{-7}$ s^{-1} was selected as a reference strain-rate with reference $\sigma'^{rr}_{p0} = 52$ kPa. A value of Poisson's ratio $\upsilon' = 0.2$ was assumed. The slopes of critical state line $M_c = 1.25$ and $M_e = 1.05$ were measured from triaxial test results (see Fig. 12(b)). The viscous parameters, N and μ, can be calculated using Eq. (21). As discussed earlier, the anisotropic parameter ω can be directly calculated using Eq. (13) based on test results of step-changed drained triaxial test (see Fig. 8). However, because such test is not available on St. Herblain clay, the parameter $\omega = 80$ was determined by curve fitting from the undrained triaxial extension test at a strain-rate of 1%/h by Zentar (1999) (see Fig. 12(b)). The selected values of parameters are summarized in Table 1, which were used for test simulations.

For the case of simulations obtained by the "isotropic model", the calibrated values of parameters with $\alpha_0 = 0$ and $\omega = 0$ were used.

It is noted that all simulations for undrained tests were carried out by performing anisotropic consolidation stage (not shown in figures) followed by undrained shearing stage, as laboratory test procedures.

(2) *Determined from 24 h oedometer tests (see Fig. 12(c))*

Due to the variation of the samples of St. Herblain, the values of κ and λ from this test are different from those obtained from CRS test. The value of $C_{\alpha e}$ was obtained from the time–settlement curve for the loading increment from 69 to 132 kPa (see Fig. 12(d)). The reference time $\tau_r = 24$ h with a reference preconsolidation pressure $\sigma'^{rr}_{p0} = 39$ kPa was obtained from this test. The values of $C_{\alpha e}$ and τ_r were used to calculate the viscous parameters N and μ using Eq. (24). The determination of other parameters is the same as that based on CRS test. The calibrated parameters are shown in Table 1.

6.2. One-dimensional creep behaviour

For simulating one-dimensional creep test by using finite element code PLAXIS v8, the value of permeability is needed. The soil permeability $k_0 = 2 \times 10^{-9}$ m/s and the coefficient $c_k = 1.15$ (the parameter for the evolution of the permeability k with void ratio e by using $k = k_0 10^{(e-e_0)/c_k}$) were obtained from the time–settlement curves of oedometer test. Fig. 12(d) shows good agreement between the simulation based on 24 h test and experiment for one-dimensional creep behaviour, as expected by the parameter calibration.

For the simulation based on CRS test, the $\sigma'^{rr}_{p0} = 45$ kPa was used instead of 52 kPa, because the depth of the sample of 24 h test is 1.2 m less than that of the sample of CRS test (keeping the same OCR $= \sigma'^{rr}_{p0}/\sigma'_{v0}$). The simulation underestimated the vertical strain due to different values of κ and λ selected from different tests. The difference is very small, and the predicted $C_{\alpha e}$ is equal to $(\lambda - \kappa)/N$. Therefore, the one-dimensional creep behaviour can be predicted by parameters obtained from CRS test.

6.3. One-dimensional strain-rate behaviour

The CRS oedometer test conducted by Rangeard (2002) was described in the previous section. For the simulation based on 24 h test, the $\sigma'^{rr}_{p0} = 45$ kPa instead of 39 kPa was suggested due to different depth of samples (keeping the same OCR).

Fig. 13(a) shows good agreement between the simulations based on CRS test and experiment for one-dimensional strain-rate behaviour, as expected by the parameter calibration. The simulations based on 24 h test by the model incorporating anisotropy are also in reasonable agreement with the experimental data. The isotropic model predicted well the vertical stress, but overpredicts the horizontal stress. Also for the stress path in Fig. 13(b), the anisotropic model predicted a stress path followed by the Jaky's formula, while the stress ratio predicted by the isotropic model is much lower. The comparisons suggest that anisotropy is sufficient to be considered for accurate predictions.

Fig. 14 shows the model predictive ability for the strain-rate effect on the apparent preconsolidation pressure, i.e., linear relationship between the preconsolidation pressure and the strain-rate, as expected by the parameter calibration. From a practical view point, there is no difference in prediction as to whether the parameters are determined from CRS tests or conventional oedometer tests.

6.4. Undrained triaxial strain-rate behaviour

The undrained triaxial compression tests with multistage constant strain-rates on St. Herblain clay (Rangeard, 2002) are used for model evaluation. The test was conducted at a strain-rate varying from 0.1 to 10%/h after a consolidation stage of 7 days.

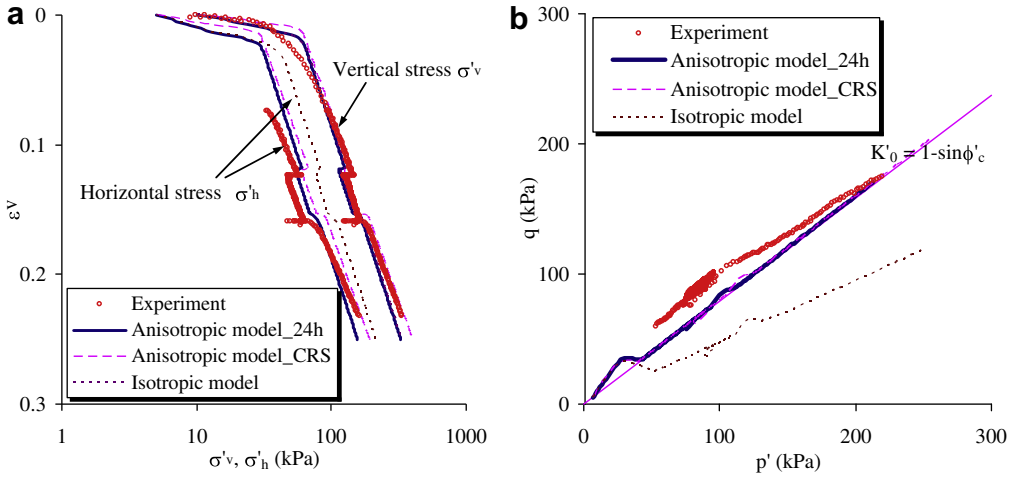

Fig. 13. CRS oedometer test on St. Herblain clay. Experimental data versus simulations for (a) stress–strain, and (b) for effective stress path.

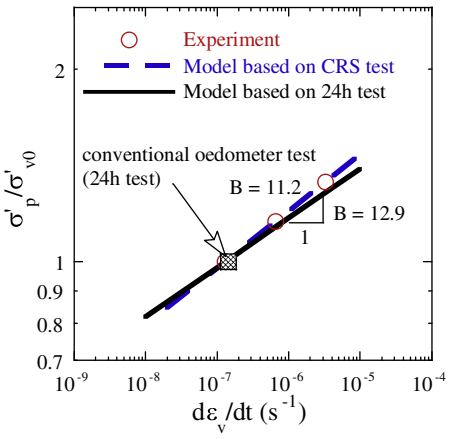

Fig. 14. CRS oedometer test on St. Herblain clay. Experimental data versus simulations for apparent preconsolidation pressure by strain-rate.

Fig. 15 shows the comparison between the predictions and measurements. Both isotropic and anisotropic models based on both CRS and 24 h tests can reasonably predict the strain-rate triaxial behaviour, although some discrepancies were found between predicted and measured results which is possibly due to the elastic anisotropy during its sedimentation and variation of natural samples. If the inherent anisotropy of elastic stiffness is included (by introducing the ratio between the horizontal and vertical Young's modulus $n = E_h/E_v = 0.3$ with $\upsilon_{vv} = \upsilon_{vh}/\sqrt{n}$ and $2G_{vh} = \sqrt{n}E_v/(1+\upsilon_{vh})$, see details in Graham and Houlsby (1983)), and if the secondary compression coefficient $C_{\alpha e} = 0.022$ is assumed (instead of 0.034), the model would give much better predictions, as shown in Fig. 15(c) and (d).

The undrained triaxial extension test at a constant strain-rate of 1%/h on the same clay by Zentar (1999) was simulated using both sets of parameters. As shown in Fig. 12(b), the anisotropic model gives noticeably improved predictions for the stress path in triaxial extension.

6.5. Undrained triaxial creep behaviour

For this evaluation, we have carried out an undrained triaxial creep test with two-stage deviatoric stress levels on the same clay sample. The sample was anisotropically consolidated under $K_0 = 0.54$ for 14 days. After that, the first vertical stress increment $\Delta\sigma'_1 = 5$ kPa was applied instantaneously while keeping the confining pressure constant. After 18 days, the second loading increment $\Delta\sigma'_1 = 5$ kPa was applied instantaneously and kept constant until the rupture of the clay sample.

Fig. 16(a) shows the comparison of predicted and measured curves of the axial strain versus time for the two applied stress levels. The isotropic model fails to give a reasonable prediction. The predictions are improved by incorporating the feature of anisotropic model (based on both CRS and 24 h tests). In terms of pre-

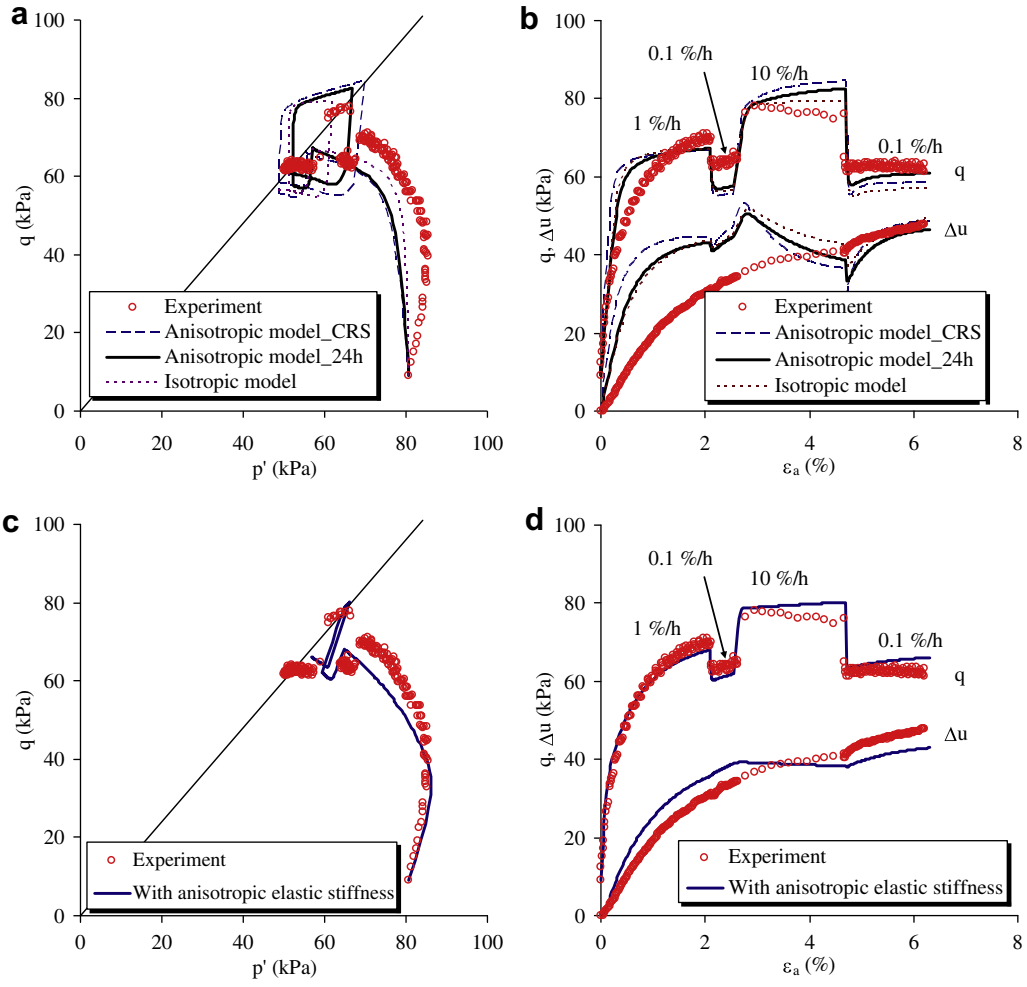

Fig. 15. CRS undrained triaxial test on St. Herblain clay. Experimental data versus simulations for (a) – (b) models with isotropic elastic stiffness and (c) – (d) anisotropic model with inherent anisotropy of elastic stiffness.

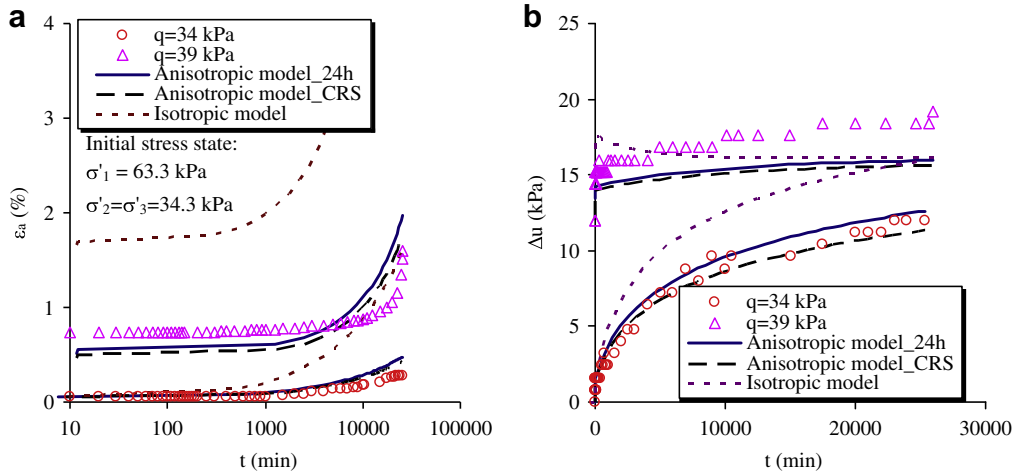

Fig. 16. Undrained triaxial creep test on St. Herblain clay. Experimental data versus simulations for (a) axial strain by time and (b) excess pore pressure by time.

dicted pore pressures (Fig. 16(b)), the predictions are reasonable for anisotropic model while the predictions are either overestimated the excess pore pressure or unreasonably estimated a decreasing pore pressure. This demonstrates that anisotropy is needs to be considered in order to capture undrained creep behaviour of natural soft clay.

7. Conclusions

Both overstress and creep models have limitations to simulate the stress–strain-time behaviour of natural soft clay. The limitations are as follows:

(a) For conventional overstress models, the determination of viscosity parameters requires tests at very low loading-rate which are not an easy task and feasible to be conducted for geotechnical practice. Thus, the initial size of static yield surface is usually assumed. Consequently, values of viscosity parameters are dependent of this assumed value.
(b) Isotropic creep models by Kutter and Sathialingam (1992), Vermeer and Neher (1999) and Yin et al. (2002) are only suitable for reconstituted soils under fixed loading conditions. The consideration of the initial anisotropy and its evolution due to irrecoverable straining can improve the model performance for natural soft clay, as investigated by Leoni et al. (2008).
(c) The isotropic creep models by Vermeer and Neher (1999) and Yin et al. (2002) and their anisotropic versions by Leoni et al. (2008) and Zhou et al. (2005) predict an unrealistic strain-softening behaviour for undrained triaxial tests, and the stress path cannot overpass the critical state line for normally consolidated clay, which are in conflict with the experimental evidence for soft clay.

In the present approach, we removed these limitations by incorporating the following concepts and formulations:

(a) The conventional overstress model was extended using the concept of reference surface instead of the static yield surface, which allows viscoplastic strain-rate occurring whatever the stress state is inside or outside of the reference surface. A scaling function based on the experimental results of constant strain-rate oedometer tests was adopted for the convenience of parameters determination.
(b) The new model adopted the formulations of a yield surface with kinematic hardening and rotation (Wheeler et al., 2003) so that it is capable of simulating the inherent and induced anisotropy.
(c) The viscoplastic volumetric strain-rate follows the critical state concept, which becomes zero when the stress state reaches the critical state line. This consideration overcomes the problems (strain-softening and stress path underpass CSL) revealed in creep models.

It is attractive that the proposed model can capture the anisotropic and viscous behaviours without any additional test, compared to the Modified Cam Clay model, required for parameter determination.

The experimental verification is presented with reference to the tests on St. Herblain clay. The database includes 24 h standard oedometer test, oedometer test at constant strain-rate with the measurement of lateral stress, undrained triaxial tests at constant strain-rate, and undrained triaxial creep tests. Test simulations were carried out using the proposed anisotropic model together with the reduced isotropic version. Different approaches of parameter determination, i.e., based on the CRS test and based on the 24 h test, were examined. All comparisons between predicted and measured results have demonstrated that the proposed model can successfully reproduce the anisotropic and viscous behaviours of natural soft clays under different loading conditions. Both CRS and 24 h tests can be alternatively used for the determination of model parameters.

Acknowledgments

The work presented was sponsored by the Academy of Finland (Grant 210744) and carried out as part of a Marie Curie Research Training Network "Advanced Modelling of Ground Improvement on Soft Soils (AMGISS)" supported the European Community through the programme "Human Resources and Mobility".

Appendix A

The detailed definitions of some terms used in this paper are described in this section.

- Deviatoric stress tensor

$$\sigma'_d = \begin{bmatrix} \sigma'_x - p' \\ \sigma'_y - p' \\ \sigma'_z - p' \\ \sqrt{2}\tau_{xy} \\ \sqrt{2}\tau_{yz} \\ \sqrt{2}\tau_{zx} \end{bmatrix} = \begin{bmatrix} \frac{1}{3}(2\sigma'_x - \sigma'_y - \sigma'_z) \\ \frac{1}{3}(-\sigma'_x + 2\sigma'_y - \sigma'_z) \\ \frac{1}{3}(-\sigma'_x - \sigma'_y + 2\sigma'_z) \\ \sqrt{2}\tau_{xy} \\ \sqrt{2}\tau_{yz} \\ \sqrt{2}\tau_{zx} \end{bmatrix} \tag{A.1}$$

- Deviatoric strain tensor (incremental)

$$d\varepsilon_d = \begin{bmatrix} \frac{1}{3}(2d\varepsilon_x - d\varepsilon_y - d\varepsilon_z) \\ \frac{1}{3}(-d\varepsilon_x + 2d\varepsilon_y - d\varepsilon_z) \\ \frac{1}{3}(-d\varepsilon_x - d\varepsilon_y + 2d\varepsilon_z) \\ \sqrt{2}d\varepsilon_{xy} \\ \sqrt{2}d\varepsilon_{yz} \\ \sqrt{2}d\varepsilon_{zx} \end{bmatrix} = \begin{bmatrix} \frac{1}{3}(2d\varepsilon_x - d\varepsilon_y - d\varepsilon_z) \\ \frac{1}{3}(-d\varepsilon_x + 2d\varepsilon_y - d\varepsilon_z) \\ \frac{1}{3}(-d\varepsilon_x - d\varepsilon_y + 2d\varepsilon_z) \\ \frac{1}{\sqrt{2}}d\gamma_{xy} \\ \frac{1}{\sqrt{2}}d\gamma_{yz} \\ \frac{1}{\sqrt{2}}d\gamma_{zx} \end{bmatrix} \tag{A.2}$$

- Deviatoric fabric tensor

$$\alpha_d = \begin{bmatrix} \frac{1}{3}(2\alpha_x - \alpha_y - \alpha_z) \\ \frac{1}{3}(-\alpha_x + 2\alpha_y - \alpha_z) \\ \frac{1}{3}(-\alpha_x - \alpha_y + 2\alpha_z) \\ \sqrt{2}\alpha_{xy} \\ \sqrt{2}\alpha_{yz} \\ \sqrt{2}\alpha_{zx} \end{bmatrix} = \begin{bmatrix} \alpha_x - 1 \\ \alpha_y - 1 \\ \alpha_z - 1 \\ \sqrt{2}\alpha_{xy} \\ \sqrt{2}\alpha_{yz} \\ \sqrt{2}\alpha_{zx} \end{bmatrix} \tag{A.3}$$

where the components of the fabric tensor have the property $\frac{1}{3}(\alpha_x + \alpha_y + \alpha_z) = 1$.

A scalar value of α can then be defined as:

$$\alpha = \sqrt{3/2(\alpha_d : \alpha_d)} \tag{A.4}$$

For cross-anisotropic material $\alpha_x = \alpha_z$ and $\alpha_{xy} = \alpha_{yz} = \alpha_{zx} = 0$.

For an initial value α, the initial values of α_{ij} are calculated as follows:

$$\begin{cases} \alpha_x = \alpha_z = 1 - \frac{\alpha_0}{3} \\ \alpha_y = 1 + \frac{2\alpha_0}{3} \\ \alpha_{xy} = \alpha_{yz} = \alpha_{zx} = 0 \end{cases} \tag{A.5}$$

References

Adachi, T., Oka, F., 1982. Constitutive equations for normally consolidated clay based on elasto-viscoplasticity. Soils and Foundations 22 (4), 57–70.

Anandarajah, A., Kuganenthira, N., Zhao, D., 1996. Variation of fabric anisotropy of kaolinite in triaxial loading. ASCE Journal of Geotechnical Engineering 122 (8), 633–640.

Biarez, J., Hicher, P.Y., 1994. Elementary Mechanics of Soil Behaviour. Balkema, Amsterdam.

Bjerrum, L., 1967. Engineering geology of Norwegian normally-consolidated marine clays as related to settlements of building. Géotechnique 17 (2), 81–118.

Britto, A.M., Gunn, M.J., 1987. Critical State Soil Mechanics Via Finite Elements. Wiley, New York.

Burland, J.B., 1990. On the compressibility and shear strength of natural clays. Géotechnique 40 (3), 329–378.

Diaz Rodriguez, J.A., Leroueil, S., Alemán, J.D., 1992. Yielding of Mexico City clay and other natural clays. Journal of Geotechnical Engineering 118 (7), 981–995.

Fodil, A., Aloulou, W., Hicher, P.Y., 1997. Viscoplastic behaviour of soft clay. Géotechnique 47 (3), 581–591.

Graham, J., Houlsby, G.T., 1983. Anisotropic elasticity of a natural clay. Géotechnique 33 (2), 165–180.

Graham, J., Crooks, J.H.A., Bell, A.L., 1983. Time effects on the stress–strain behaviour of natural soft clays. Géotechnique 33 (3), 327–340.

Hicher, P.Y., Wahyudi, H., Tessier, D., 2000. Microstructural analysis of inherent and induced anisotropy in clay. Mechanical Cohesive-Frictional Materials 5 (5), 341–371.

Hinchberger, S.D., Rowe, R.K., 2005. Evaluation of the predictive ability of two elastic–viscoplastic constitutive models. Canadian Geotechnical Journal 42 (6), 1675–1694.

Karstunen, M., Koskinen, M., 2008. Plastic anisotropy of soft reconstituted clays. Canadian Geotechnical Journal 45 (3), 314–328.

Katona, M.G., 1984. Evaluation of viscoplastic cap model. ASCE Journal of Geotechnical Engineering 110 (8), 1106–1125.

Kimoto, S., Oka, F., 2005. An elasto-viscoplastic model for clay considering destructuralization and consolidation analysis of unstable behaviour. Soils and Foundations 45 (2), 29–42.

Kutter, B.L., Sathialingam, N., 1992. Elastic–viscoplastic modelling of the rate-dependent behaviour of clays. Géotechnique 42 (3), 427–441.

Leoni, M., Karstunen, M., Vermeer, P.A., 2008. Anisotropic creep model for soft soils. Géotechnique 58 (3), 215–226.

Leroueil, S., Kabbaj, M., Tavenas, F., Bouchard, R., 1985. Stress–strain–strain-rate relation for the compressibility of sensitive natural clays. Géotechnique 35 (2), 159–180.

Leroueil, S., Kabbaj, M., Tavenas, F., 1988. Study of the validity of a $\sigma'v$–εv–$d\varepsilon v/dt$ model in site conditions. Soils and Foundations 28 (3), 13–25.

Mabssout, M., Herreros, M.I., Pastor, M., 2006. Wave propagation and localization problems in saturated viscoplastic geomaterials. International Journal for Numerical Methods in Engineering 68 (4), 425–447.

Mesri, G., Godlewski, P.M., 1977. Time and stress–compressibility interrelationship. ASCE Journal of the Geotechnical Engineering 103 (5), 417–430.

Nash, D.F.T., Sills, G.C., Davison, L.R., 1992. One-dimensional consolidation testing of soft clay from Bothkennar. Géotechnique 42 (2), 241–256.

Oka, F., 1992. A cyclic elasto-viscoplastic constitutive model for clay based on the non-linear-hardening rule. In: Pande, G.N., Pietruszczak, S. (Eds.), Proceedings of the Fourth International Symposium on Numerical Models in Geomechanics, Swansea, vol. 1, Balkema, pp. 105–114.

Oka, F., Adachi, T., Okano, Y., 1986. Two-dimensional consolidation analysis using an elasto-viscoplastic constitutive equation. International Journal for Numerical and Analytical Methods in Geomechanics 10 (1), 1–16.

Oka, F., Kodaka, T., Kim, Y.-S., 2004. A cyclic viscoelastic–viscoplastic constitutive model for clay and liquefaction analysis of multi-layered ground. International Journal for Numerical and Analytical Methods in Geomechanics 28 (2), 131–179.

Perzyna, P., 1963. The constitutive equations for work-hardening and rate sensitive plastic materials. Proceedings of the Vibration Problems Warsaw 3, 281–290.

Perzyna, P., 1966. Fundamental problems in viscoplasticity. Advances in Applied Mechanics 9, 243–377.

Rangeard, D., 2002. Identification des caractéristiques hydro-mécaniques d'une argile par analyse inverse des essais pressiométriques. Thèse de doctorat, Ecole Centrale de Nantes et l'Université de Nantes.

Roscoe, K.H., Burland, J.B., 1968. On the Generalized Stress–Strain Behaviour of 'Wet' Clay. Engineering Plasticity. Cambridge University Press, Cambridge. pp. 553–609.

Rowe, R.K., Hinchberger, S.D., 1998. Significance of rate effects in modelling the Sackville test embankment. Canadian Geotechnical Journal 35 (3), 500–516.

Shahrour, I., Meimon, Y., 1995. Calculation of marine foundations subjected to repeated loads by means of the homogenization method. Computers and Geotechnics 17 (1), 93–106.

Sheahan, T.C., Ladd, C.C., Germaine, J.T., 1996. Rate-dependent undrained shear behaviour of saturated clay. ASCE Journal of the Geotechnical Engineering 122 (2), 99–108.

Sheng, D., Sloan, S.W., Yu, H.S., 2000. Aspects of finite element implementation of critical state models. Computational Mechanics 26, 185–196.

Tavenas, F., Leroueil, S., 1977. Effects of stresses and time on yielding of clays. In: Proceedings of the Ninth ICSMFE, vol. 1, pp. 319–326.

Vaid, Y.P., Campanella, R.G., 1977. Time-dependent behaviour of undisturbed clay. ASCE Journal of the Geotechnical Engineering 103 (7), 693–709.

Vermeer, P.A., Neher, H.P., 1999. A soft soil model that accounts for creep. In: Proceedings of the Plaxis Symposium on Beyond 2000 in Computational Geotechnics, Amsterdam, pp. 249–262.

Wheeler, S.J., Näätänen, A., Karstunen, M., Lojander, M., 2003. An anisotropic elasto-plastic model for soft clays. Canadian Geotechnical Journal 40 (2), 403–418.

Yin, J.H., Cheng, C.M., 2006. Comparison of strain-rate dependent stress–strain behaviour from K_0-consolidated compression and extension tests on natural Hong Kong Marine deposits. Marine Georesources and Geotechnology 24 (2), 119–147.

Yin, Z.Y., Hicher, P.Y., 2008. Identifying parameters controlling soil delayed behaviour from laboratory and in situ pressuremeter testing. International Journal for Numerical and Analytical Methods in Geomechanics 32 (12), 1515–1535.

Yin, J.H., Zhu, J.G., Graham, J., 2002. A new elastic–viscoplastic model for time-dependent behaviour of normally and overconsolidated clays: theory and verification. Canadian Geotechnical Journal 39 (1), 157–173.

Yin, Z.-Y., Chang, C.S., Hicher, P.Y., Karstunen, M., 2009. Micromechanical analysis of kinematic hardening in natural clay. International Journal of Plasticity 25 (8), 1413–1435.

Zentar, R., 1999. Analyse inverse des essais pressiométriques, application à l'argile de Saint-Herblain. Thèse de doctorat, Ecole Centrale de Nantes et l'Université de Nantes.

Zhou, C., Yin, J.H., Zhu, J.G., Cheng, C.M., 2005. Elastic anisotropic viscoplastic modeling of the strain-rate-dependent stress–strain behaviour of K_0-consolidated natural marine clays in triaxial shear tests. ASCE International Journal of Geomechanics 5 (3), 218–232.